Distributed brain networks for anticipatory modulation of human response times

Ashwin Ramayya (ashwinramayya@gmail.com)
University of Pennsylvania
Vivek Buch
Stanford University
Andrew Richardson
University of Pennsylvania https://orcid.org/0000-0002-4752-3867
Timothy Lucas
University of Pennsylvania
Joshua Gold
University of Pennsylvania https://orcid.org/0000-0002-6018-0483

Article

Keywords: simple sensory-motor behaviors, human brain, brain networks, human response times

Posted Date: August 30th, 2021

DOI: https://doi.org/10.21203/rs.3.rs-841658/v1

Abstract

Simple sensory-motor behaviors that engage the central nervous system can provide a window onto key building blocks of cognition, such as via response times (RTs) that are sensitive to learned, task-dependent expectations. However, our understanding of the mechanisms that support these cognitive effects on behavior, particularly in the human brain, remains limited, in part because of a major disconnect between the simple algorithmic models often used to describe behavioral patterns and the complex neural dynamics associated with sensory-motor and cognitive information processing in the brain. Here we used quantitative behavioral analyses and intracranial recordings from patients with medically refractory epilepsy to identify specific, computationally defined components of expectation-dependent RT variability in the brain. Behaviorally derived models based on abstracted motor-preparatory processes provided useful, low-dimensional descriptions of the underlying neural computations. These descriptions did not have clear local neural representations, including in motor-preparatory regions, but instead were evident in certain emergent network-wide neural response properties that reflected task-relevant neural activity patterns with diverse timing, form, and anatomical locations. Our results illustrate the complex mapping between algorithmic and implementation-level descriptions of flexible neural information processing and identify specific, distributed networks the brain uses to combine expectations with sensory input to guide behavior.

Main Text

Since the first systematic measures of response times (RTs) in the late 19th century, RT variability has been recognized as a fundamental property of behavior *(1,2)*. Even for simple tasks, such as responding as quickly as possible to an easily identifiable visual stimulus with a predetermined movement (e.g., a button press), RTs are far slower than expected based on neural transmission latencies *(3)* and are highly variable across individuals *(4)*. This additional, variable processing time is not evident in purely peripheral reflexes *(5)* and instead reflects contributions of the central nervous system to sensory-motor processing that include a sensitivity to learned expectations *(6–9)*. However, the exact nature of these contributions, including where and how they are represented in the brain, is not well understood *(10)*.

A major set of open questions concerns if and how algorithmic descriptions of these higher-order contributions to sensory-motor processing relate to the underlying neural signals. One such set of algorithms are found in "rise-to-bound" models in which a stimulus-initiated latent process rises until reaching a threshold value, generating a motor response *(11–17)*. In these models, which can provide good fits to RT behavior and are compelling cognitive building blocks because of their close ties to statistical decision theory *(18,19)*, trial-to-trial variability in the pre-stimulus starting point and the rising process governs anticipatory and reactive forms of RT variability, respectively *(13)*. Correlates of these modeled effects have been identified in several motor-preparatory brain regions, including activity patterns that map directly *(22,26)* or indirectly *(23,24,30)* onto model dynamics. However, these findings have provided only a limited understanding of the underlying brain signals, because previous studies that identified RT-related representations have either had high resolution but local scope (e.g., invasive recordings in animals that typically target individual neurons in specific motor or sensory-motor brain regions thought to be relevant to a particular task but neglect potential contributions by the rest of the brain; *22–24*) or more global scope but much lower resolution (e.g., brain-wide human imaging studies that lack the temporal resolution to identify all but the coarsest RT modulations, or EEG that lacks the spatial resolution to distinguish local versus global representations; *25–29;* although see *30*).

To overcome these limitations, we studied 23 patients implanted with intraparenchymal electrodes for intracranial encephalography (iEEG) evaluation of medically refractory epilepsy as they performed a simple RT task with a variable foreperiod delay *(2)* (Fig. 1, table S1). Each trial began with the presentation of a visual target on a computer screen that changed color after either 500 ms or 1500 ms ("short" versus "long" foreperiod delay, randomly interleaved). Subjects were instructed to respond via button press as soon as they noticed the color change ("stimulus"). We defined correct responses as those that occurred within 1000 ms after stimulus and measured RT as the time between stimulus and response. On correct trials, subjects were provided with visual feedback immediately after the response. We defined anticipatory false alarms as those that occurred after target but before stimulus onset and measured anticipatory RT as the time between target and response. On false-alarm trials (and trials with no response within 1000 ms), subjects were shown a blank screen for ~ 2.5 s before the next trial began.

We observed three main behavioral effects (Fig. 1). First, subjects showed stochastic RT variability for both delay conditions (median per-subject RT inter-quartile range = 67 ms for short-delay and long-delay trials). Second, subjects showed anticipatory delay-related adjustments in RT, with, on average, a tendency to respond with faster (paired *t*-test, $t(22) = 5.57$, $p < 0.001$) and less variable RTs ($t(22) = 2.4$, $p = 0.03$) on long versus short delay trials (mean RT range = 354–595 ms and 323–529 ms on short- and long-delay trials, respectively). Third, subjects showed a wide range of anticipatory false-alarm rates (range 1.7%–58%) that were correlated with faster RTs ($r = 0.47$, $p = 0.02$) on long delay trials. Subjects rarely showed anticipatory false alarms on short delay trials (range 0–7.8%).

We modelled RT behavior using a pair of "rise-to-bound" processes that assumed that motor responses occur when a latent variable that increases in value linearly and deterministically over time reaches a threshold level or "bound" *(13;* fig. S1). The first process was triggered by the onset of the target and accounted for anticipatory false alarms. The second process was triggered by the color change and accounted for correct responses. We fit the model to data from each subject separately, with two free parameters to account for delay-related changes in behavior (Fig. 1e; we used this form of the model to distinguish delay-dependent RT modulations with and without associated false alarms; other possible model parameterizations are detailed in the Supplemental Text): 1) anticipation bias, which governed the overall probability of generating anticipatory false alarms (which tended to occur on only long-duration trials); and 2) the difference in variance of the reactive rise-to-bound process between short and long duration trials ("Δ variance", which is equivalent to certain coupled changes in the rate-of-rise and distance-to-bound in the model) *(13)*. The model provided a good fit to the subjects' RT distributions (R^2 mean = 0.83, range = 0.55–0.99, fig. S1) and showed that: 1) stochastic, trial-by-trial RT variability could be captured by stochastic variability in the rate of rise of the rise-to-bound process; 2) delay-related changes in RTs could be captured by two independent anticipatory influences on RTs, anticipation bias (with captured correlated

changes in faster RTs and more false alarms on long delay trials; fig S1d,e) and Δ variance (which captured changes in RTs that were not related to false alarms; fig. S1c,d); and 3) anticipatory false alarm rates could be captured by the anticipation bias term ($r = 0.76$, $p < 0.001$).

To identify neural substrates of these behavioral patterns, we measured intracranial high-frequency activity (HFA, 70–200 Hz), which is a reliable surrogate of local neural population spiking activity *(31–33)*, from 2,609 bipolar pairs of intraparenchymal depth electrodes widely distributed throughout the brain in 23 patients (Figs. 2a, S2a). The HFA from many of these electrodes exhibited task-related modulation patterns, including differences by delay condition (Figs. 2b, S2b, c). We compared across-subject differences in RT behavior, quantified via the rise-to-bound model fits, to global neural state dynamics measured separately for each subject (Fig. 2, S3). These global network measures represent distributed patterns of correlated neural activity across all electrodes from a given subject as trajectories in a high-dimensional neural-state space, where each dimension represents the temporally dynamic, task-dependent activity measured from each electrode *(34)* (fig. S3, Supplemental text).

Two features of these high-dimensional trajectories were related systematically the two parameters of the rise-to-bound model that accounted for delay-related RT differences, on a subject-by-subject basis. First, subjects with greater differences between pre-stimulus brain states just before the short- versus long-delay cues (“pre-stimulus discriminability,” which is conceptually related to the starting point in the rise-to-bound model) tended to have higher Δ variance (i.e., they tended to respond more quickly and with more variability on long-delay trials, but without an increase in false alarms; *rho* = 0.58; FDR-corrected $p = 0.021$; Fig. 2c). That is, this measure of global pre-stimulus neural activity was related to the modeled change in sensory-motor processing that led to anticipation-dependent RT differences that were independent of false alarms. Second, subjects with brain-state trajectories between stimulus and response onset on long- versus short-delay trials (“post-stimulus trajectory”, which is conceptually reminiscent of the rate of rise in the model) that were more direct tended to have larger anticipation biases (i.e., a greater tendency to respond more quickly on long-delay trials, with an associated increase in false-alarms; *rho* = 0.59, FDR-corrected $p = 0.021$; Figs. 2d; see also Supplemental text and Fig. S4 for additional relationships). That is, this measure of global post-stimulus neural activity was related to the modeled anticipatory influences on RTs that resulted in increased false alarms.

To relate these widespread representations of anticipatory RT processing to more localized neural activity patterns, we identified potentially relevant electrodes as those with activity that exhibited modulations by stochastic RT variability and/or delay condition. Specifically, we measured the task-driven “activation function” of the neural population near each electrode by averaging z-scored HFA time-locked to target onset and motor response (fig. S2). We then identified all electrodes that had activation functions that were modulated by either stochastic (delay-independent) RT variability, after accounting for transient sensory- and motor-driven responses, or the delay condition (fig. S5). In general, correlates of both RT variability (Figs. 3, S6) *(30)* and delay condition (fig. S7) *(10)* were widespread across the brain, heterogeneous (most brain regions contained electrodes that showed opposing direction of modulation; i.e., increases and decreases in activity with faster RTs), and dynamic (distinct electrodes showed modulations over the course of the trial).

Given the heterogeneity of task-related neural representations across these electrodes, we performed data-driven unsupervised clustering to identify neural populations that showed similar activity modulations related to stochastic RT variability and delay condition (figs. S8–12, Supplemental Text). We identified 20 such clusters that could be distinguished by various anatomical and functional properties, not used by the clustering algorithm (Figs. 3c; fig. S8; table S7; subsequent results were qualitatively consistent with other clustering levels, Supplemental Text). Figure 3c shows one such cluster (cluster 6) with activity modulations by RT that occurred primarily before stimulus onset (higher activity corresponded to faster RTs), followed by a largely RT-independent rate of rise before the motor response. This cluster contained electrodes that were found largely in perirolandic (premotor-related) regions, but this localization was the exception, not the rule. Instead, most clusters included electrodes that were distributed widely throughout the brain, despite having similar task-driven activity patterns. The different clusters were also distinguished by different patterns of selectivity for RT and/or delay condition that occurred at various times during each trial and different relationships to other task-relevant factors including error feedback, anticipatory responses, and spatial selectivity (figs. S8, S11, S12, table S7). Thus, these clustering analyses showed a much more widespread anatomical distribution than just premotor areas that have been the targets of many previous studies and a much greater diversity of activity patterns than the kinds of joint modulations by delay condition and stochastic RT variability expected from simple versions of the rise-to-bound model (fig. S1) *(21,22,24)*.

To relate these diverse and distributed activity patterns to behaviorally relevant RT processing, we assessed the relative contribution of each cluster to the across-subject correlations between differences in RT behavior and global neural state dynamics shown in Fig. 2. Specifically, we quantified the relative contribution of each cluster as the change in the given correlation after excluding electrodes from that cluster (Fig. 4). We also performed complementary analyses that excluded electrodes by brain region, not cluster, to assess more directly the anatomical localization of behaviorally relevant modulations. We found that both the pre-stimulus discriminability (Fig. 2c) and post-stimulus trajectory (Fig. 2d) results were not dependent on any single electrode group but rather reflected widespread network-wide phenomena that were observed across functionally heterogeneous electrode groups and brain regions (Fig. 4).

Notably, the pre-stimulus (Fig. 2c) and post-stimulus (Fig. 2d) modulations engaged different sets of functionally and anatomically heterogeneous clusters. Specifically, the correlation between Δ variance and pre-stimulus discriminability was most strongly influenced by: 1) cluster 11, which exhibited activity modulations that included a faster post-stimulus rate-of-rise on long versus short delay trials and relatively strong spatial selectivity, consistent with its prominent localization in occipital cortex; and 2) cluster 9, which exhibited activity modulations that included faster post-stimulus rate-of-rise during faster versus slower RTs and frequent correlations with the timing of anticipatory false alarms, with a prominent localization in insula (Fig. 4a; fig. S12), and generally by electrodes in ventral visual stream white matter and perirolandic regions (Fig. 4b). In contrast, the correlation between anticipation bias and post-stimulus trajectory was most strongly influenced by: 1) cluster 2, which exhibited activity modulations that included an increased pre-response rate-of-rise on short versus long delay trials, with a prominent localization in insula; and 2) cluster 7, which exhibited activity modulations that included an increased pre-response rate-of-rise preceding faster versus slower RTs, with a prominent localization in occipital cortex (Fig. 4c; fig. S11), and electrodes located in cingulate and fronto-temporal white matter (Fig. 4d). However, none of these clusters or anatomically defined groups alone made a statistically reliable contribution to either correlation (permutation procedure, FDR corrected p’s > 0.2) emphasizing the distributed nature of the underlying neural signals.

Our results illustrate the complex mapping between algorithmic rise-to-bound models of sensory-motor behavior and human brain activity. We identified brain-wide dynamics that were related conceptually to the two delay-dependent terms in our model, suggesting that behaviorally derived algorithms can provide a low-dimensional summary of relevant neural computations. However, the relationship between these global dynamics and their constituent local neural activity patterns was not nearly as straightforward. In some cases, local neural signals could be mapped directly onto certain components of the rise-to-bound model (e.g., RT-dependent activity that appears to rise to a particular level just before each motor response found in premotor regions; Fig. 3d), which is consistent with other reports of similar representations in the human brain *(21–23,26)*. However, these rise-to-bound-like signals comprised only a subset of neural activity that was relevant for anticipatory modulation of behavioral RTs. Instead, behaviorally relevant activity patterns were diverse in form and location and in many cases did not show straightforward mappings onto components of the model. These results are consistent with previous findings showing heterogeneous representations of RT modulations within a single brain region *(23)* and across multiple brain regions *(20,30)*. They also show that neural computations that can have relatively simple form that matches aggregated neural activity can emerge from a multitude of heterogeneous, distributed, and elementary computations carried out by complex neural systems *(20)*, thus demonstrating the need for new models and approaches to help bridge the gap between behavior, algorithms, and the complex neural systems that implement them *(37–39)*.

Our results also provide support for the emerging view that even simple sensory-motor processing engages widespread brain networks (*35,36)*, and suggest that a primary function of these distributed, heterogeneous, and dynamic representations is to integrate reactive sensory-motor transformations with diverse forms of anticipatory processing *(7–9)*. We showed that two forms of behaviorally relevant anticipatory processing, one related to early responses (false alarms) and the other related to additional delay-related changes in RT, modulate distinct network dynamics on a global scale that encompass a diversity of localized neural activity patterns throughout the brain. More generally, such widespread networks linking anticipatory and reactive processing may provide a window onto the basic evolutionary advantages conferred by a complex central nervous system, which ensures that our actions are not purely reflexive but instead make use of information integrated over multiple timescales to accelerate, delay, or otherwise modulate behavioral responses in a manner that allows us to thrive in a dynamic and uncertain world.

Conclusions

Anticipatory influences of RT variability during simple sensory-motor behavior can be explained by an algorithmic model of abstracted motor-preparatory signals. However, neural correlates of these anticipatory influences are evident in widespread neural dynamics across heterogeneous neural populations and not limited to motor-preparatory signals that directly resemble model dynamics.

Declarations

Acknowledgments: Drs. Michael Kahana, Daniel Yoshor, Michael Beauchamp, Tahra Eissa, Matthew Nassar, Long Ding and and Kareem Zaghloul for helpful feedback on the manuscript. Cameron Brandon, Everett Prince, John Bernabei, Jacqueline Boccanfuso, and Joel Stein for technical assistance in data collection.

Funding: National Institutes of Health grant 6T32NS091006 (AGR)

Author contributions:

Conceptualization: AGR, VB, AR, TL, and JIG

Methodology: AGR, VB, AR, JIG

Formal Analysis: AGR

Investigation: VB, AR, TL

Visualization: AGR, JIG

Funding acquisition: AR, TL, JIG

Project administration: AR

Supervision: TL, JIG

Writing – original draft: AGR, JIG

Writing – review & editing: AGR, AR, TL, JIG

Competing interests: Authors declare that they have no competing interests.

Data and materials availability: All data and code included in the study will be made available upon request.

Supplementary Materials

Materials and Methods

Supplementary Text

Figs. S1 to S12

Tables S1 to 7

References And Notes

1. J.M. Cattell, The time taken up by cerebral operations. *Mind* ***11.42*** (1886)
2. R.D. Luce, *Response Times: Their Role in Inferring Elementary Mental Organization.* (Oxford University Press, 1986)
3. B. Sabatini, W. Regehr, Timing of neurotransmission at fast synapses in the mammalian brain. *Nature.* ***384*** (1996)
4. J. Carlson, C. Jensen, K. Widaman, Reaction time, intelligence, and attention. *Intelligence*. ***7*** (1983)
5. C.J.M. Frijns, D.M. Laman, M.A.J. Van Duijn, H. Van Duijn Normal values of patellar and ankle tendon reflex latencies. *Clin Neurol Neurosurg.* ***99*** (1997)
6. R. Naatanen, P. Niemi, Foreperiod and simple reaction time. *Psychol Bull.* ***89*** (1981)
7. H. von Helmholtz, *Treatise on Physiological Optics* (Voss, Hamburg, 1867).
8. P. Dayan, G. E. Hinton, R.M. Neal, The Helmholtz machine. *Neural Comput.* ***7*** (1995).
9. K. Friston, The free-energy principle: a unified brain theory? *Nature reviews neuroscience*. ***11*** (2010)
10. A.C. Nobre, F. van Ede, Anticipated moments: temporal structure in attention. *Nat Rev Neurosci.* ***19*** (2018)
11. M. Stone, Models for choice-reaction time. *Psychometric.* ***25*** (1960)
12. R. Ratcliff, P.L. Smith, S.D. Brown, G. McKoon, Diffusion Decision Model: Current Issues and History. *Trends Cogn Sci.* ***20*** (2016)
13. I. Noorani, R.H.S. Carpenter, The LATER model of reaction time and decision. *Neurosci Biobehav Rev.* ***64*** (2016)
14. R.H.S. Carpenter, M.L.L. Williams, Neural computation of log likelihood in control of saccadic eye movements. *Nature.* ***377*** (1995)
15. S.D. Brown, A. Heathcote, The simplest complete model of choice response time: Linear ballistic accumulation. *Cogn Psychol.* ***57*** (2008)
16. R. Ratcliff. A theory of memory retrieval. *Psychol Rev.* ***85*** (1978)
17. M. Usher, J.L. McClelland, The time course of perceptual choice: The leaky, competing accumulator model. *Psychol Rev.* ***108*** (2001)
18. A. Wald, Sequential Tests of Statistical Hypotheses. *Ann Math Stat.* ***16*** (1945)
19. I.J. Good, Studies in the history of probability and statistics. XXXVII A. M. Turing's statistical work in World War II. *Biometrika.* ***66*** (1979)
20. R.G. O'Connell, M.N. Shadlen, K.F. Wong-Lin, S.P. Kelly, Bridging Neural and Computational Viewpoints on Perceptual Decision-Making. *Trends Neurosci.* ***41*** (2018)
21. J.I. Gold, M.N. Shadlen, The neural basis of decision making. *Annu Rev Neurosci.* ***30*** (2007)
22. D. Hanes, J. Schall, Neural control of voluntary movement initiation. *Science.* ***274*** (1996)
23. R.P. Heitz, J.D. Schall. Neural Mechanisms of Speed-Accuracy Tradeoff. *Neuron.* ***76*** (2012)
24. C.K. Hauser, D. Zhu, T.R. Stanford, E. Salinas, Motor selection dynamics in FEF explain the reaction time variance of saccades to single targets. *Elife.* ***7*** (2018)
25. M.D. Fox, A.Z. Snyder, J.L. Vincent, M.E. Raichle. Intrinsic Fluctuations within Cortical Systems Account for Intertrial Variability in Human Behavior. *Neuron.* ***56*** (2007)
26. R.G. O'Connell, P.M. Dockree, S.P. Kelly, A supramodal accumulation-to-bound signal that determines perceptual decisions in humans. *Nat Neurosci.* ***15*** (2012)
27. R. Ratcliff, M.G. Philiastides, P. Sajda, R.M. Shiffrin, Quality of evidence for perceptual decision making is indexed by trial-to-trial variability of the EEG. *PNAS.* ***106*** (2009)
28. E. Callaway, C.L. Yeager, Relationship between reaction time and electroencephalographic alpha phase. *Science.* ***132*** (1960)
29. R.E. Dustman, E.C. Beck, Phase of alpha brain waves, reaction time and visually evoked potentials. *Electroencephalogr Clin Neurophysiol.* ***18*** (1965)
30. S.E. Paraskevopoulou, W.G. Coon, P. Brunner, K.J. Miller, G. Schalk, Within-subject reaction time variability: Role of cortical networks and underlying neurophysiological mechanisms. *NeuroImage.* ***237*** (2021)
31. J.R. Manning, J. Jacobs, I. Fried, M.J. Kahana, Broadband Shifts in Local Field Potential Power Spectra Are Correlated with Single-Neuron Spiking in Humans. *J Neurosci.* ***29*** (2009)
32. S. Ray, J.H.R. Maunsell, Different Origins of Gamma Rhythm and High-Gamma Activity in Macaque Visual Cortex. *PLoS Biol.* ***9*** (2011)
33. A. Dubey, S. Ray, Cortical Electrocorticogram (ECoG) is a local signal. *J Neurosci* ***39*** (2019)
34. S. Vyas, M.D. Golub, D. Sussillo, K.V. Shenoy, Computation through Neural Population Dynamics. *Annu Rev Neurosci.* ***43*** (2020)
35. M.M. Mesulam, From sensation to cognition. *Brain.* ***121*** (1998)
36. J. Gonzalez-Castillo, Z.S. Saad, D.A. Handwerker, S.J. Inati, N. Brenowitz, P.A. Bandettini, Whole-brain, time-locked activation with simple tasks revealed using massive averaging and model-free analysis. *PNAS.* ***109*** (2012)
37. K.F. Wong, X.J. Wang, A recurrent network mechanism of time integration in perceptual decisions. *J Neurosci.* ***26*** (2006)
38. R. Bogacz, K. Gurney, The basal ganglia and cortex implement optimal decision making between alternative actions. *Neural Comput.* ***19*** (2007)
39. G.R. Yang, X.J. Wang, Artificial Neural Networks for Neuroscientists: A Primer. *Neuron.* ***107*** (2020)

40. A.G. Ramayya, A.I. Yang, V.P. Buch, J.F. Burke, A.G. Richardson, C. Brandon, J.M. Stein, K.A. Davis, H.I. Chen, A. Proekt, M.B. Kelz, B. Litt, J.I. Gold, T.H. Lucas, Theta Synchrony Is Increased near Neural Populations That Are Active When Initiating Instructed Movement. *eNeuro.* ***8*** (2021)
41. S. Liu, J. Parvizi, Cognitive refractory state caused by spontaneous epileptic high-frequency oscillations in the human brain. *Science translational medicine.* ***11*** (2019)
42. B.B. Avants, N.J. Tustison, G. Song, P.A. Cook, A. Klein, J.C. Gee, A reproducible evaluation of ANTs similarity metric performance in brain image registration. *Neuroimage.* ***54*** (2011)
43. B. Landman, S. Warfield, MICCAI workshop on multi-atlas labeling. In: Medical image computing and computer assisted intervention conference. (2012)
44. S. Warrington, K.L. Bryant, A.A. Khrapitchev, J. Sallet, M. Charquero-Ballester, G. Douaud, S. Jbabdi, R.B. Mars, S.N. Sotiropoulos, XTRACT - Standardised protocols for automated tractography in the human and macaque brain. *Neuroimage* ***217*** (2020)
45. J.Mazziotta, A.Toga, A.Evans, P.Fox, J.Lancaster, K.Zilles, R.Woods, T.Paus, G.Simpson, B.Pike, C.Holmes, L.Collins, P.Thompson, D.MacDonald, M.Iacobon Gallagher, S.Geyer, L.Parsons, K.Narr, N.Kabani, G.Le Goualher, D.Boomsma, T.Cannon, R.Kawashima, B.Mazoyer, A probabilistic atlas and reference system for the human brain: International Consortium for Brain Mapping (ICBM) *Philos Trans R Soc London Ser B Biol Sci.* ***356*** (2001)
46. Y. Benjamini, Y. Hochberg, Controlling the False Discovery Rate: A Practical and Powerful Approach to Multiple Testing. *J R Stat Soc Ser B.* ***57*** (1995)

Figures

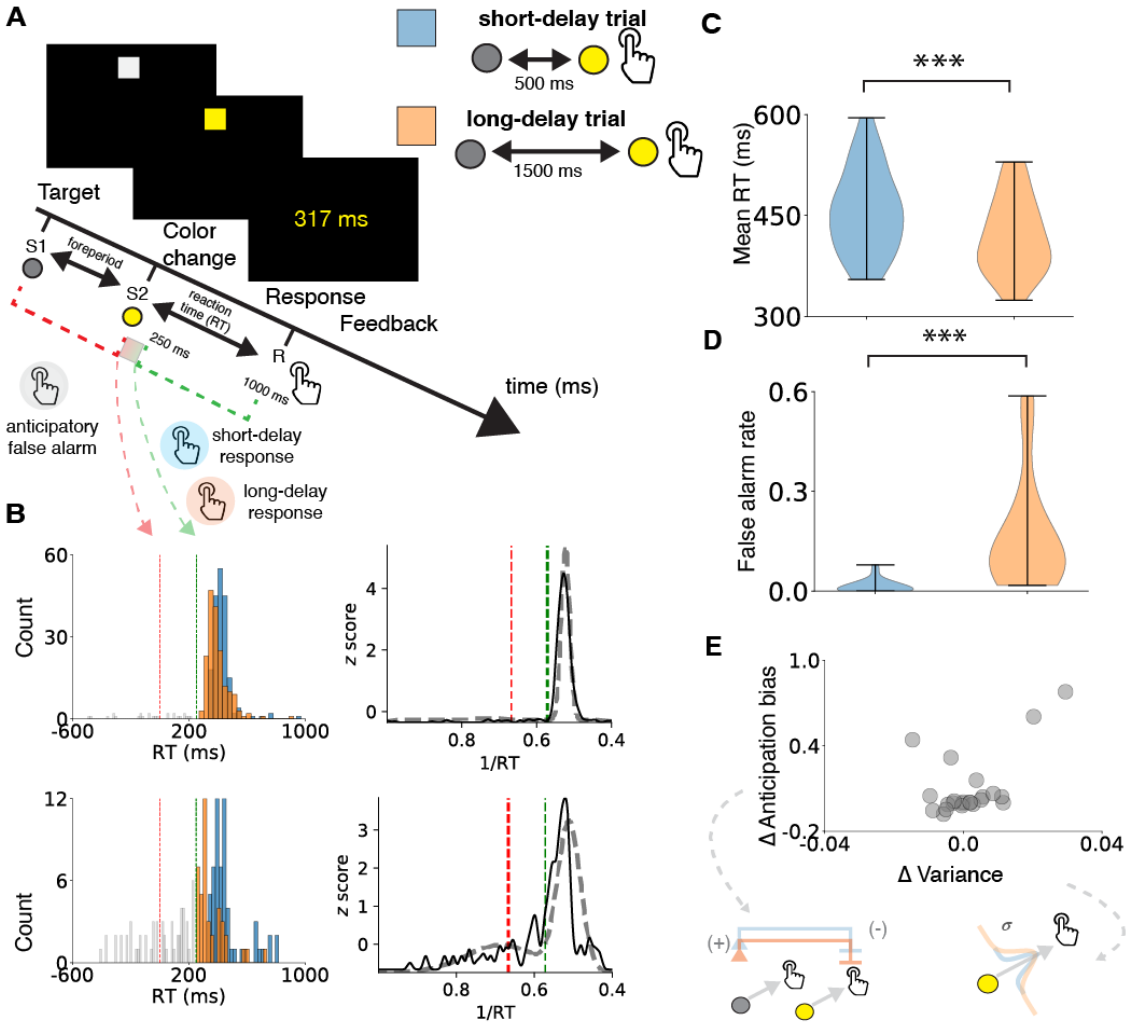

Figure 1

RTs from a simple detection paradigm reflect two distinct forms of anticipatory processing. (A) Stimulus-detection task with variable foreperiod delay. (B) Left, RT distributions from two example subjects (top and bottom rows). Red line indicates stimulus onset, green vertical line indicates 250 ms after stimulus onset (the fast-response threshold). Grey histogram indicates timing of premature responses, blue and orange histograms indicate timing of responses on short- and long-delay trials, respectively. Right, reciprocal RT distributions (13) (black) and rise-to-bound model fits (dashed grey line). (C, D) Violin plots showing distributions of mean RTs (C) and anticipatory false alarm rates (D) on short- (blue) and long-delay (orange) trials for all 23 subjects. (E) Best-fitting values of the two delay-sensitive model parameters: anticipatory bias (ordinate, positive values imply more false alarms on long-versus short-delay trials) and Δ

variance (abscissa, positive values imply an increase in across-trial variance of the stimulus-driven rising process on long- versus short-delay trials). Each circle corresponds to data from a single subject.

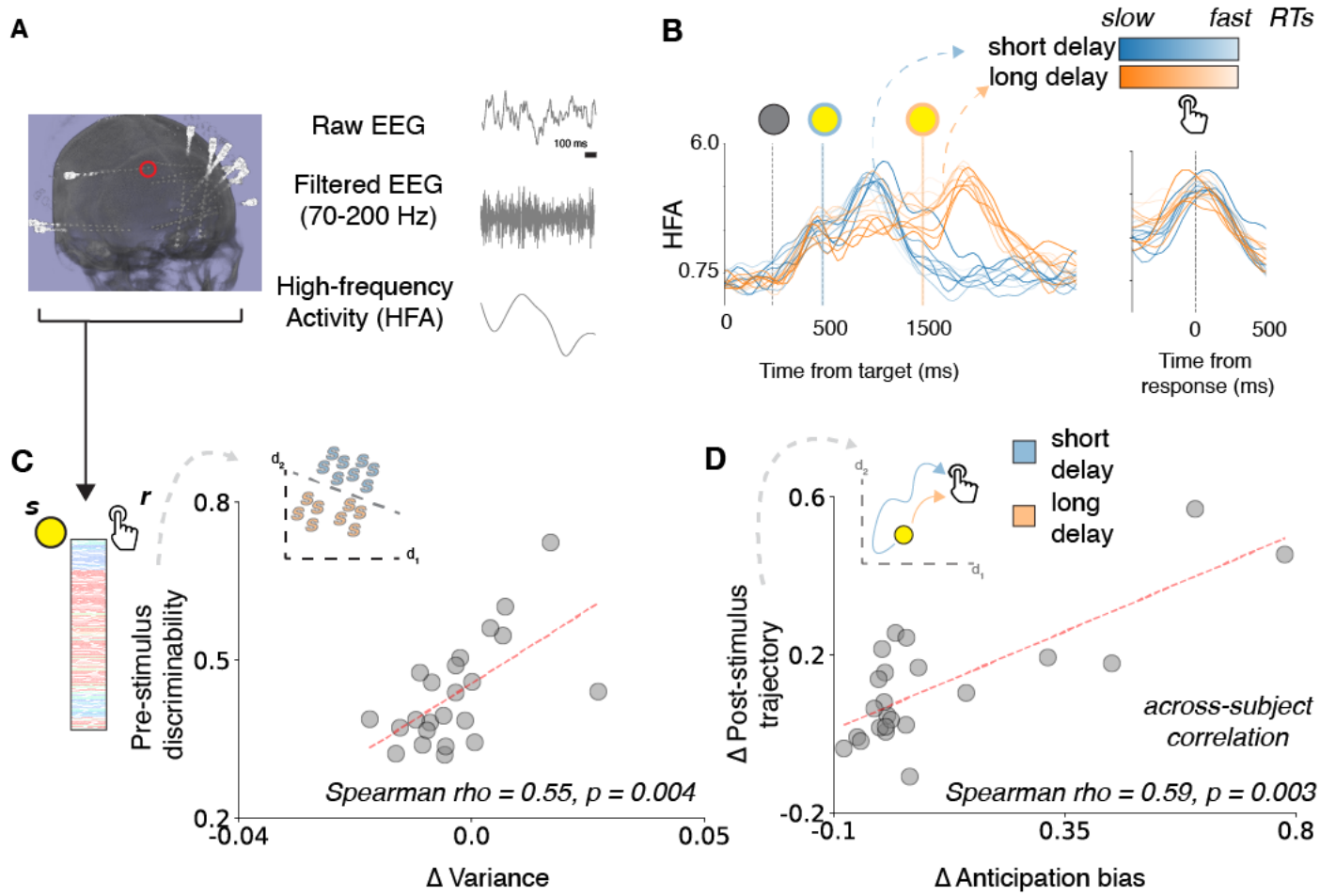

Figure 2

Anticipatory RT biases are reflected in widespread neural dynamics. (A) Extracting high frequency activity (HFA,70–200 Hz power) from intraparenchymal depth electrodes as an estimate of local spiking (fig. S2). (B) Task-driven responses of local neural activity measured at the electrode indicated in A (red circle; average z-scored HFA locked to target and response), plotted separately for short- (blue) and long- (orange) delay trials and binned by stochastic RT percentile (10 bins; lighter shading indicates faster RTs; fig. S3). Vertical lines indicate time of target onset (grey), short-delay color change (blue), and long-delay color change (orange), respectively. (C) Across-subject relationship between behaviorally derived Δ variance (abscissa) and discriminability between widespread neural activity prior to stimulus presentation ("pre-stimulus discriminability" on the ordinate; see inset and fig. S3) compared between short- and long-duration trials. (D) Across-subject relationship between behaviorally derived Δ anticipation bias (abscissa) and widespread neural dynamics between stimulus and response ("Δ post-stimulus trajectory" on the ordinate; see inset and fig. S3) compared between short- and long-duration trials. Each circle in C and D corresponds to data from a single subject.

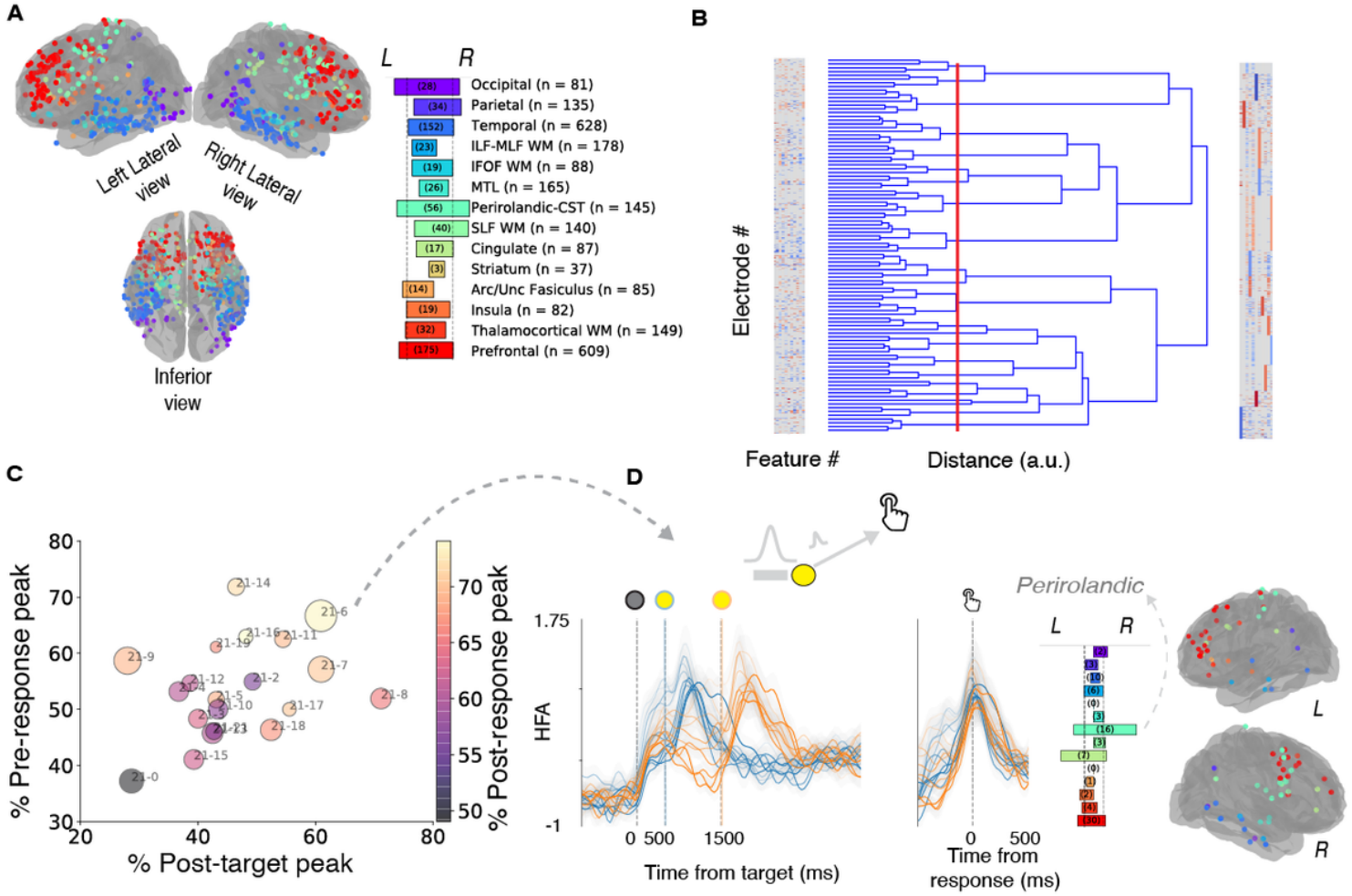

Figure 3

Distributed representations of RT variability. (A) Anatomical distribution of all electrodes that showed correlations with stochastic RT variability (non-parametric test, $p < 0.05$). Brain plots show electrode locations of RT-modulated electrodes using standardized anatomical coordinates, colored by brain region as indicated to the right. Horizontal bar plots indicate proportions of RT-modulated electrodes in each region (width of bar plot) and across hemisphere (L/R, indicated by offset relative to center). Vertical dashed lines indicate uniformly distributed proportions (figs. S6, S7). (B) Electrode clustering based on similar modulation by stochastic RT or foreperiod delay ($p < 0.05$, non-parametric tests). (Left) colormap representing feature matrix across all electrodes, which are randomly arranged (each row represents an electrode, each column indicates correlation with RT or delay modulation across various time intervals; fig. S5, red indicates positive correlation, blue indicates negative correlation, grey indicates no relation, organized by subject). (Middle) Dendrogram representing results clustering algorithm as electrodes are grouped together into a single cluster (left to right). Red line indicates level of grouping used to identify electrode clusters (based on an objective function; fig. S8). (Right) Feature matrix re-organized based on similar RT and delay modulations at clustering level indicated by red line in middle panel. (C) Scatterplot of 20 functionally distinct clusters that we identified, which could be distinguished based on their responses just following target onset (abscissa) and just prior to (ordinate) and just following (colors, as indicated to the right) the behavioral response. Size of circles indicate degree of anatomical localization (larger circles are more localized, based on χ^2 statistics comparing anatomical distribution to uniform). (D) Example cluster resembling rise-to-bound activity (6 in fig. S11). Left, average target- and response-locked activation functions, plotted as in Fig. 2B. Right, anatomical distributions of electrodes in cluster 6, plotted as in A.

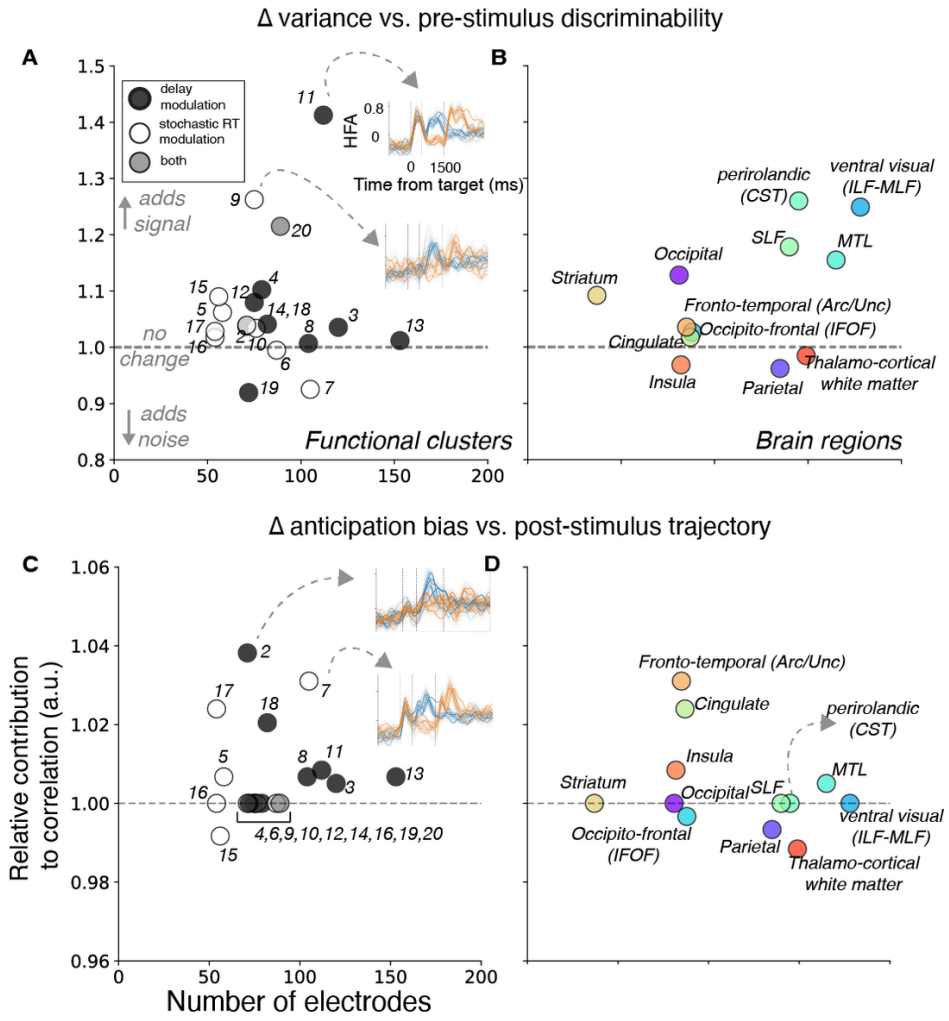

Figure 4

Anticipatory RT biases reflect diverse, distributed neural activity patterns. (A) Scatterplot showing the relative contributions of each functionally defined cluster to the across-subject correlation between Δ variance and pre-stimulus discriminability shown in Fig. 2C. Abscissa shows the number of electrodes in each cluster. Ordinate shows the fraction change in rho after removing the cluster (or brain region); a value >1 or <1 implies that including the given cluster increased or decreased the correlation, respectively. Shading indicates clusters with predominantly delay-related modulation (black), stochastic RT modulation (white), or both (gray) defined based on frequency of modulation (figs. S11,S12). Insets show activation functions associated with the two most influential clusters, plotted as in Fig. 2B. (B) Same as left panel, except for brain regions colored as in Fig 3A. (C, D) Same as A, B, but for the across-subject correlation between Δ anticipation bias and post-stimulus trajectory shown in Fig. 2D.

Supplementary Files

This is a list of supplementary files associated with this preprint. Click to download.

- RamaEtalantReactsupp.docx